

RESEARCH ARTICLE

Virtual Synchronous Generator Control Strategy of Grid-Forming Matrix Converter for Renewable Power Generation

JIANWEI ZHANG^{1,2}, (Member, IEEE), HUIDONG WANG^{1,2},
GUANGCHEN LIU^{1,2}, (Member, IEEE), GUIZHEN TIAN^{1,2},
MARCO RIVERA^{3,4}, (Senior Member, IEEE), AND PATRICK WHEELER³, (Fellow, IEEE)

¹College of Electric Power, Inner Mongolia University of Technology, Hohhot 010080, China

²Engineering Research Center of Large Energy Storage Technology, Minister of Education, Inner Mongolia University of Technology, Hohhot 010080, China

³Power Electronics, Machines and Control Research Group, Faculty of Engineering, University of Nottingham, NG7 2RD Nottingham, U.K.

⁴Laboratory of Energy Conversion and Power Electronics (LCEEP), Universidad de Talca, Talca 3460000, Chile

Corresponding author: Jianwei Zhang (zjwzachary@outlook.com)

This work was supported in part by Inner Mongolia Natural Science Foundation under Grant 2024MS05041, in part by the Program for Young Talents of Science and Technology in Universities of Inner Mongolia Autonomous Region under Grant NJYT22082, in part by the Basic Scientific Research Expenses Program of Universities Directly under Inner Mongolia Autonomous Region under Grant JY20220092 and Grant JY20230009, in part by the Projects from the University of Nottingham under Grant ENNOBLE-R02401 and Grant IRCF 24932270, in part by the Fondecyt Regular Project under Grant 1220556, in part by the Anid/Anillo Project under Grant ATE220023 and Grant FOVI230169, and in part by the FONDAP SERC Chile under Grant 1522A0006.

ABSTRACT Matrix converters (MC) have been considered for applications in renewable power generation and microgrids. However, similar to other power electronic converter-interfaced power generation systems, the MC-interfaced system cannot provide inertia or damping effect to support the grid's frequency or voltage. To improve the inertia and damping effect of the MC-interfaced distributed generation system and realize the grid-friendly connection of new energy power generation, a virtual synchronous generator (VSG) control strategy suitable for the MC-interfaced system is proposed. Aiming at the problem that the system frequency in the traditional VSG cannot be restored to the nominal value after the load power fluctuations, the VSG secondary frequency control strategy is introduced. To ensure a smooth grid connection, a synchronization control strategy based on virtual power has been designed. An experimental validation platform was built and the experimental results verify the correctness and effectiveness of the proposed control strategies for a grid-forming MC.

INDEX TERMS Damping, inertia, matrix converter, secondary frequency control, virtual synchronous generator.

I. INTRODUCTION

Many countries around the world have set goals for net zero emissions of greenhouse gas. Renewable power generation is a key technology to help achieve these goals. Therefore, a large number of renewable energy power generation systems will be connected to the power grid, which requires numerous power electronic converters [1], [2], [3]. With the increasing penetration of new energy and wide application

The associate editor coordinating the review of this manuscript and approving it for publication was Snehal Gawande¹.

of power electronic converters, the system equivalent inertia constant significantly decreases. Literature [4] has shown that from 1996 to 2016, the proportion of new energy generation in Europe increased from 14% to 31%, while the system equivalent inertia constant decreased by about 20%. Reduced system inertia will lead to a larger rate of change and deviation of frequency [5], [6]. In addition, the new energy power generation systems are usually operated in the maximum power tracking mode and they do not exhibit the inertia and damping characteristics observed in traditional synchronous generators. Consequently, they are incapable

of actively providing the necessary voltage and frequency support for the power grid, which seriously threatens the stability of the power grid. Therefore, it is particularly important to enhance the inertia and damping of new energy power generation systems.

To address the issue of low inertia and weak damping in a power system with a high percentage of new energy, Zhong et al. have proposed and studied the concept of the virtual synchronous generator (VSG) [7]. VSG has been widely investigated for interface converters to improve the performance of renewable power generation systems and achieve friendly grid integration [8], [9], [10]. Current research on VSG control technology is mainly carried out based on DC/AC converters [3]. In literature [11], VSG has been applied to control DC/AC inverters in conventional PV systems, so the grid-following PV systems are transformed into grid-forming systems, thus providing inertial support for the grid. In [10], VSG has been investigated in battery and ultra-capacitor combined energy storage systems to compensate for the power fluctuation in new energy generation systems and provide support for grid frequency. In [12], a VSG-based adaptive cooperative control strategy has been proposed in a photovoltaic power generation system equipped with battery storage to ensure grid frequency stability while maximizing the use of photovoltaic power.

However, some electrical power generation systems have an AC output nature and it is necessary to utilize back-to-back converters to realize AC/AC conversion. Some researchers have studied the VSG control technique for the back-to-back converters in wind power generation systems [13], [14], [15]. VSG can enable wind power generation systems to exhibit dynamic characteristics similar to synchronous generation and provide inertia support to the grid while maintaining the maximum power point tracking capability. The VSG in wind power generation systems is usually implemented on the grid-side DC/AC converter which is a part of a back-to-back converter. However, back-to-back converters contain large electrolytic capacitors in the DC link. These capacitors are usually large, heavy, and require maintenance, and they also require DC voltage control and cause energy loss [13]. In contrast, a matrix converter (MC) can realize direct AC/AC conversion without a DC energy storage link. As a competitive alternative solution to a back-to-back converter, the MC provides advantageous features such as compactness, lightweight, controllable input power factor, sinusoidal waveform, four-quadrant operation, and high efficiency. Therefore, MCs can generally be used in applications where the back-to-back converter is used. More specifically, MC can be used as the interface converter between AC-source distributed generation systems, such as wind power generation systems and flywheel energy storage systems, or microgrids and electrical power grids [16].

MCs have been widely researched in renewable power generation applications. Similar to other power electronic converters used in renewable and distributed power generation systems, the traditional grid-following control strategy of

MC cannot provide the desired frequency and voltage support to the grid. However, the VSG control of MC is seldom reported in the literature, not to mention the control of the grid-forming MC. In [17] the authors have proposed a VSG control technique with MC as the main topology to realize direct AC/AC conversion. However, a hysteresis band controller has been used, and it is prone to generating harmonics with a wide spectral distribution, which can make the filter design complex. In [18] a novel space vector algorithm to control MC is described, but the algorithm is complex and the grid-connection control is not considered. In [19] the authors have proposed a VSG-based grid-connected control strategy for MC and the power delivered to the grid is effectively regulated. However, the input power factor control is not considered. The above literature has shown that the VSG control of MC has important research value. However, none of them considers the overall operation process of the MC-based VSG power generation system.

The main work of this paper is summarized as follows. (1) The concept of grid-forming MC is put forward and the basic principle and control strategy of VSG are analyzed for grid-forming MC. (2) The secondary frequency regulation strategy is incorporated into the VSG control to remove the steady-state error of the system output frequency in the conventional VSG scheme. (3) To achieve smooth grid connection, a virtual power-based grid synchronization control strategy without using PLL is designed. (4) The simulation and experimental results are presented to demonstrate the feasibility and effectiveness of the proposed control strategy in islanded, switching and grid-connected modes.

II. VSG FUNDAMENTALS

VSG control technology can use the electromechanical equation of the synchronous generator in the control loop of the power electronic converter so that the inertia, damping, primary frequency control, and primary voltage regulation characteristics of the synchronous generator are incorporated in the converter control. In this way, the converter-interfaced renewable power generation system can mimic the traditional synchronous generator and exhibit favorable support to the grid. The VSG active power-frequency control is based on the rotor motion process of a synchronous generator, and its mathematical equation is expressed by

$$\begin{cases} J \frac{d\omega}{dt} = \frac{P_{\text{ref}} - P_e}{\omega_0} - D\Delta\omega \\ \omega = \frac{d\theta}{dt} \end{cases} \quad (1)$$

where J is the virtual inertia; P_{ref} is the reference active power; P_e is the actual output active power; D is the damping coefficient; ω is the angular velocity; ω_0 is the rated angular velocity; $\Delta\omega = \omega - \omega_0$; θ is the electrical angle. The VSG active power-frequency control block diagram is established according to (1) and is shown in Fig. 1.

The VSG reactive power-voltage control is based on the excitation regulation process of a synchronous generator.

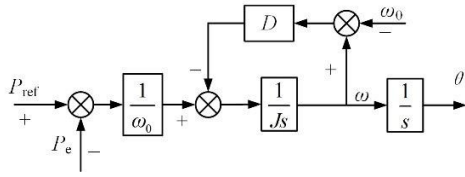


FIGURE 1. VSG active power-frequency control block diagram.

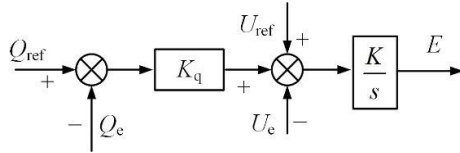


FIGURE 2. VSG reactive power-voltage control block diagram.

The synchronous generator adjusts the terminal voltage and output reactive power of the synchronous generator by controlling the excitation current. Referring to the control idea in a synchronous generator, VSG realizes the control of system output voltage and reactive power by controlling virtual electromotive force E . According to the droop relationship between voltage and reactive power, and the electromagnetic transient characteristics of synchronous generator, the virtual electromotive force E of VSG is expressed as

$$E = K \int [K_q(Q_{ref} - Q_e) + (U_{ref} - U_e)] \quad (2)$$

where E is the virtual electromotive force; K is the gain factor of the reactive power controller; K_q is the reactive power droop coefficient; Q_{ref} is the reference reactive power; Q_e is the actual output reactive power; U_{ref} is the reference output voltage; U_e is the actual output voltage. According to (2), the VSG reactive power-voltage control block diagram can be obtained as shown in Fig. 2.

III. MC STRUCTURE AND MODULATION

A. MC STRUCTURE

The MC consists of nine bidirectional switching devices arranged in a 3×3 matrix, and each bidirectional switch is composed of two semiconductor switching devices with anti-parallel diodes. The MC topology is shown in Fig. 3.

The relationship between voltage and current in MC can be expressed as:

$$\begin{bmatrix} u_A \\ u_B \\ u_C \end{bmatrix} = \begin{bmatrix} S_{Aa} & S_{Ba} & S_{Ca} \\ S_{Ab} & S_{Bb} & S_{Cb} \\ S_{Ac} & S_{Bc} & S_{Cc} \end{bmatrix} \begin{bmatrix} u_a \\ u_b \\ u_c \end{bmatrix} = S \begin{bmatrix} u_a \\ u_b \\ u_c \end{bmatrix} \quad (3)$$

$$\begin{bmatrix} i_a \\ i_b \\ i_c \end{bmatrix} = \begin{bmatrix} S_{Aa} & S_{Ab} & S_{Ac} \\ S_{Ba} & S_{Bb} & S_{Bc} \\ S_{Ca} & S_{Cb} & S_{Cc} \end{bmatrix} \begin{bmatrix} i_A \\ i_B \\ i_C \end{bmatrix} = S^T \begin{bmatrix} i_A \\ i_B \\ i_C \end{bmatrix} \quad (4)$$

where S is the switching matrix and S^T is the transpose of S . When S_{ij} ($i = A, B, C; j = a, b, c$) is 1, the corresponding switch is on, otherwise off. To prevent overcurrent caused by short-circuiting the input and overvoltage caused

TABLE 1. MC switching states.

Vector	Conducting switches	U_{oABC}	α_o	I_{iabc}	β_i
1	$S_{Aa} S_{Bb} S_{Cc}$	$h_v U_{ab}$	0	$h_i i_A$	$-\pi/6$
-1	$S_{Ab} S_{Ba} S_{Ca}$	$-h_v U_{ab}$	0	$-h_i i_A$	$-\pi/6$
+2	$S_{Ab} S_{Bc} S_{Cc}$	$h_v U_{bc}$	0	$h_i i_A$	$\pi/2$
-2	$S_{Ac} S_{Bb} S_{Cb}$	$-h_v U_{bc}$	0	$-h_i i_A$	$\pi/2$
+3	$S_{Ac} S_{Ba} S_{Ca}$	$h_v U_{ca}$	0	$h_i i_A$	$7\pi/6$
-3	$S_{Aa} S_{Bc} S_{Cc}$	$-h_v U_{ca}$	0	$-h_i i_A$	$7\pi/6$
+4	$S_{Ab} S_{Ba} S_{Cb}$	$h_v U_{ab}$	$2\pi/3$	$h_i i_B$	$-\pi/6$
-4	$S_{Aa} S_{Bb} S_{Ca}$	$-h_v U_{ab}$	$2\pi/3$	$-h_i i_B$	$-\pi/6$
+5	$S_{Ac} S_{Bb} S_{Cb}$	$h_v U_{bc}$	$2\pi/3$	$h_i i_B$	$\pi/2$
-5	$S_{Ab} S_{Bc} S_{Cb}$	$-h_v U_{bc}$	$2\pi/3$	$-h_i i_B$	$\pi/2$
+6	$S_{Aa} S_{Bc} S_{Ca}$	$h_v U_{ca}$	$2\pi/3$	$h_i i_B$	$7\pi/6$
-6	$S_{Ac} S_{Ba} S_{Cc}$	$-h_v U_{ca}$	$2\pi/3$	$-h_i i_B$	$7\pi/6$
+7	$S_{Ab} S_{Bb} S_{Ca}$	$h_v U_{ab}$	$4\pi/3$	$h_i i_C$	$-\pi/6$
-7	$S_{Aa} S_{Ba} S_{Cb}$	$-h_v U_{ab}$	$4\pi/3$	$-h_i i_C$	$-\pi/6$
+8	$S_{Ac} S_{Bc} S_{Cb}$	$h_v U_{bc}$	$4\pi/3$	$h_i i_C$	$\pi/2$
-8	$S_{Ab} S_{Bb} S_{Cc}$	$-h_v U_{bc}$	$4\pi/3$	$-h_i i_C$	$\pi/2$
+9	$S_{Aa} S_{Ba} S_{Cc}$	$h_v U_{ca}$	$4\pi/3$	$h_i i_C$	$7\pi/6$
-9	$S_{Ac} S_{Bc} S_{Ca}$	$-h_v U_{ca}$	$4\pi/3$	$-h_i i_C$	$7\pi/6$
0 _a	$S_{Aa} S_{Ba} S_{Ca}$	0	-	0	-
0 _b	$S_{Ab} S_{Bb} S_{Cb}$	0	-	0	-
0 _c	$S_{Ac} S_{Bc} S_{Cc}$	0	-	0	-
r ₁	$S_{Aa} S_{Bb} S_{Cc}$	U_{iabc}	α_i	I_{oABC}	β_o
r ₂	$S_{Aa} S_{Bc} S_{Cb}$	$-U_{iabc}$	$-\alpha_i$	I_{oABC}	$-\beta_o$
r ₃	$S_{Ab} S_{Ba} S_{Cc}$	$-U_{iabc}$	$-\alpha_i + 4\pi/3$	I_{oABC}	$-\beta_o + 2\pi/3$
r ₄	$S_{Ab} S_{Bc} S_{Ca}$	U_{iabc}	$\alpha_i + 4\pi/3$	I_{oABC}	$\beta_o + 2\pi/3$
r ₅	$S_{Ac} S_{Ba} S_{Cb}$	U_{iabc}	$\alpha_i + 2\pi/3$	I_{oABC}	$\beta_o + 4\pi/3$
r ₆	$S_{Ac} S_{Bb} S_{Ca}$	$-U_{iabc}$	$\alpha_i + 2\pi/3$	I_{oABC}	$-\beta_o + 4\pi/3$

Notes: $h_v=2/3, h_i=2/\sqrt{3}$.

by open-circuiting the output, the MC switching states must satisfy

$$\sum_{i=A,B,C} S_{ij} = 1, (j = a, b, c) \quad (5)$$

Therefore, there are 27 valid switching states in MC. Different switching states correspond to different vectors, generating different output voltages and input currents. The MC input voltage vector is defined as $U_{iabc} \angle \alpha_i$, the output voltage vector as $U_{oABC} \angle \alpha_o$, the input current vector as $I_{iabc} \angle \beta_i$, and the output current vector as $I_{oABC} \angle \beta_o$. The switching states and corresponding vectors are shown in Table 1.

B. MC MODULATION

Space vector modulation (SVM) is an effective control technique and it is used in the work described in this paper to control the MC. According to Table 1, the output voltage and input current vectors corresponding to each switching state are shown in Fig. 4.

Assuming the reference voltage vector U_{oABC} and input current vector I_{iabc} are both located in sector I in each hexagon shown in Fig. 4. U'_{oABC} , U''_{oABC} , and I'_{iabc} , I''_{iabc} are the decomposed components of the U_{oABC} and I_{iabc} and they are synthesized by the MC switching vectors with the same direction, namely +1, -3, -7 and +9. Different combinations of the switching vectors are selected based on the values of m and n , and they are summarized in Table 2.

TABLE 2. Units for magnetic properties.

	m=1	m=2	m=3	m=4	m=5	m=6
n=1	+1,-7,+9,-3,0 _c	+4,-7,+9,-6,0 _c	+4,-1,+3,-6,0 _c	+7,-1,+3,-9,0 _c	+7,-4,+6,-9,0 _c	+1,-4,+6,-3,0 _c
n=2	+9,-3,+2,-8,0 _b	+9,-6,+5,-8,0 _b	+3,-6,+5,-2,0 _b	+3,-9,+8,-2,0 _b	+6,-9,+8,-5,0 _b	+6,-3,+2,-5,0 _b
n=3	+2,-8,+7,-1,0 _a	+5,-8,+7,-4,0 _a	+5,-2,+1,-4,0 _a	+8,-2,+1,-7,0 _a	+8,-5,+4,-7,0 _a	+2,-5,+4,-1,0 _a
n=4	+7,-1,+3,-9,0 _c	+7,-4,+6,-9,0 _c	+1,-4,+6,-3,0 _c	+1,-7,+9,-3,0 _c	+4,-7,+9,-6,0 _c	+4,-1,+3,-6,0 _c
n=5	+3,-9,+8,-2,0 _b	+6,-9,+8,-5,0 _b	+6,-3,+2,-5,0 _b	+9,-3,+2,-8,0 _b	+9,-6,+5,-8,0 _b	+3,-6,+5,-2,0 _b
n=6	+8,-2,+1,-7,0 _a	+8,-5,+4,-7,0 _a	+2,-5,+4,-1,0 _a	+2,-8,+7,-1,0 _a	+5,-8,+7,-4,0 _a	+5,-2,+1,-4,0 _a

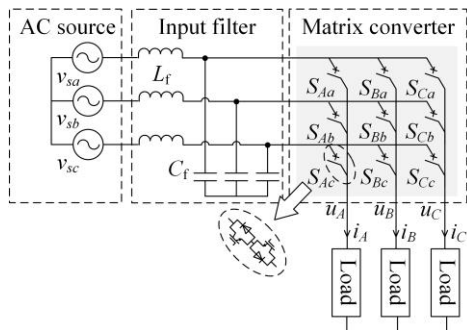


FIGURE 3. MC topology.

The duty cycles of corresponding vectors are expressed by

$$\delta^I = (-1)^{m+n} \frac{2}{\sqrt{3}} q \frac{\sin(\alpha) \sin(\beta)}{\cos(\chi_i)} \quad (6)$$

$$\delta^{II} = (-1)^{m+n+1} \frac{2}{\sqrt{3}} q \frac{\sin(\alpha) \sin(\pi/3 - \beta)}{\cos(\chi_i)} \quad (7)$$

$$\delta^{III} = (-1)^{m+n+1} \frac{2}{\sqrt{3}} q \frac{\sin(\pi/3 - \alpha) \sin(\beta)}{\cos(\chi_i)} \quad (8)$$

$$\delta^{IV} = (-1)^{m+n} \frac{2}{\sqrt{3}} q \frac{\sin(\pi/3 - \alpha) \sin(\pi/3 - \beta)}{\cos(\chi_i)} \quad (9)$$

where q is the voltage transfer ratio; $0 \leq \alpha \leq \pi/3$ is the sector angle of the desired output voltage U_{oABC} ; $0 \leq \beta \leq \pi/3$ is the sector angle of the desired input current I_{iabc} ; χ_i is the phase difference between the input current and the input voltage; and m and n are the sectors in which the output voltage and the input current are located, respectively.

The zero vector is introduced to complete the entire sampling period and its duty cycle is

$$\delta^0 = 1 - \delta^I - \delta^{II} - \delta^{III} - \delta^{IV} \quad (10)$$

According to the above descriptions, the overall control block diagram of the direct SVM of the MC is shown in Fig. 5.

IV. VSG CONTROL STRATEGY FOR MC

A. MC MODULATION

Most of the conventional VSG control strategies are implemented for inverters or back-to-back converters, and all of them require information on DC bus voltage in their control strategies. However, there is no DC link in MC, which makes its control strategy different from the conventional VSG converter [20]. The proposed MC-based VSG control strategy

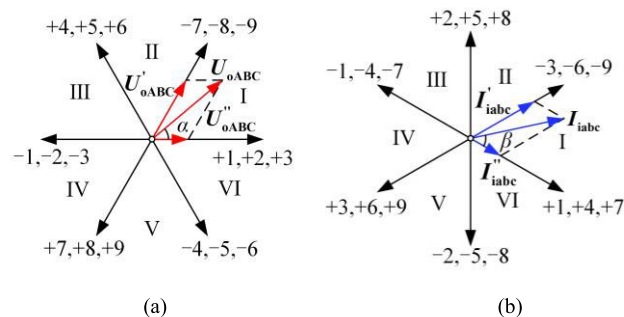


FIGURE 4. MC Output voltage vectors (a) and input current vectors (b).

mainly consists of an input current control unit, a VSG control unit, a voltage transfer ratio control unit, and a virtual power synchronization unit, as shown in Fig. 6.

The unity power factor operation at the MC input side is achieved by the input current control unit. The input source voltage phase is detected using a phase-locked loop (PLL) and used as a reference phase angle for the input current $I_{iabc} \angle \beta_i$. Direct current control based on voltage orientation is adopted, and a PI controller is utilized to control the q -axis current i_{mq} to be 0, compensating for the phase difference between the input voltage and current.

The VSG control unit generates the three-phase virtual electromotive force $E \angle \theta$ according to (1) and (2). The MC output voltage is controlled by the voltage-current double closed-loop controller. The application of the VSG technology enables the MC-based generation system to exhibit external characteristics similar to the synchronous generator.

The voltage transfer ratio control unit takes the amplitude of the reference output voltage U_{oABC} as the reference, and the system output voltage amplitude U_e as the feedback, and their difference is passed through the PI controller to control the voltage transfer ratio q .

B. VSG WITH SECONDARY FREQUENCY REGULATION

The VSG control strategy enables the MC-interfaced generation system to have the primary frequency regulation process of synchronous generators. However, there is a steady-state error in frequency regulation. Therefore, the system frequency cannot be restored to the rated value, and frequency overrun can occur when the load fluctuates significantly.

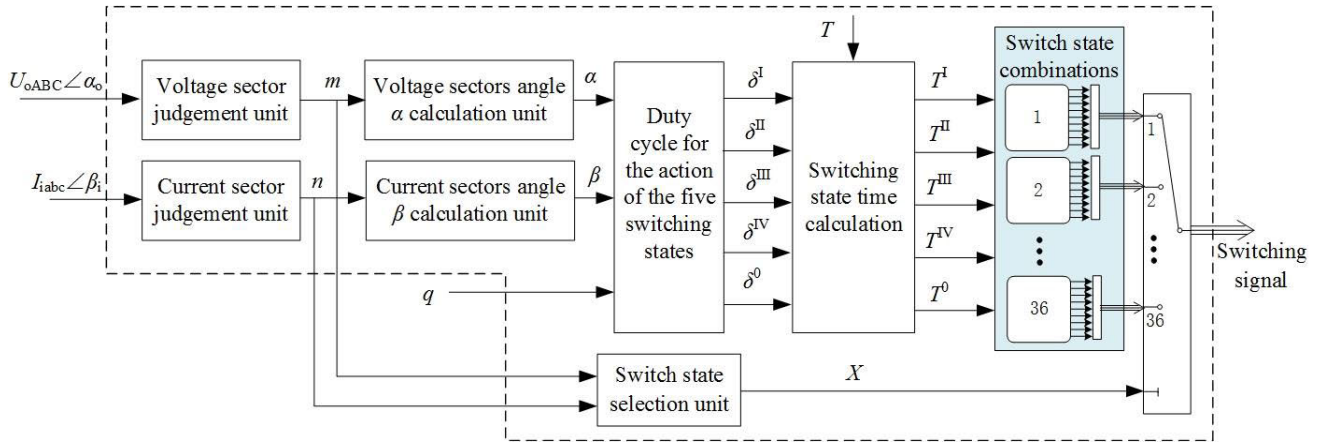


FIGURE 5. MC direct space vector control diagram.

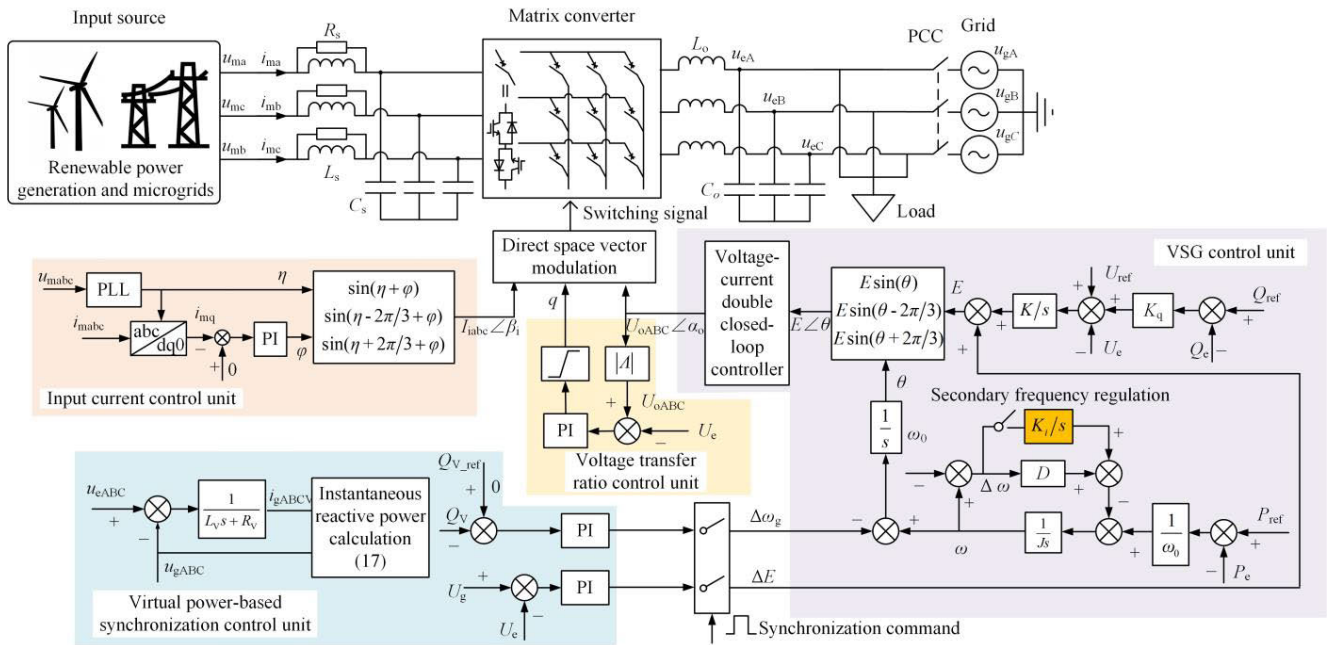


FIGURE 6. Overall control diagram of VSG for MC.

The secondary frequency regulation can be incorporated to eliminate the frequency regulation error [21].

The VSG secondary frequency modulation introduces an integral link in the active power-frequency control loop. Together with damping coefficient D , a PI controller is formed, so the steady-state error in frequency regulation can be removed. The block diagram of secondary frequency modulation is shown in Fig. 7.

According to Fig. 7, when there is a disturbance in the load in the islanded mode, the active power-frequency control can be expressed by

$$J \frac{d\Delta\omega}{dt} = \frac{P_{ref} - P_e}{\omega_0} - \left(D + \frac{K_i}{s} \right) \Delta\omega \quad (11)$$

where K_i is the integration factor. According to (11)

$$Js\Delta\omega(s) = \frac{1}{\omega_0} \Delta P(s) - \left(D + \frac{K_i}{s} \right) \Delta\omega(s) \quad (12)$$

$$\Delta\omega = -\frac{1}{\omega_0 Js^2 + D\omega_0 s + K_i\omega_0} \Delta P(s) \quad (13)$$

where $\Delta P(s) = P_{ref}(s) - P_e(s)$. According to (13), when the system power undergoes a step change, the initial and final values of the system frequency response are

$$\begin{cases} \lim_{t \rightarrow \infty} \Delta\omega = \lim_{s \rightarrow 0} s(\Delta\omega/s) = 0 \\ \lim_{t \rightarrow 0} \Delta\omega = \lim_{s \rightarrow \infty} s(\Delta\omega/s) = 0 \end{cases} \quad (14)$$

Equation (14) shows that the initial and final values of the system frequency are zero, so the VSG secondary frequency

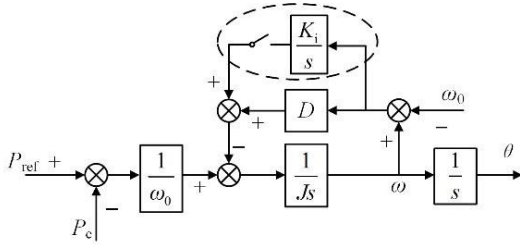


FIGURE 7. MC topology.

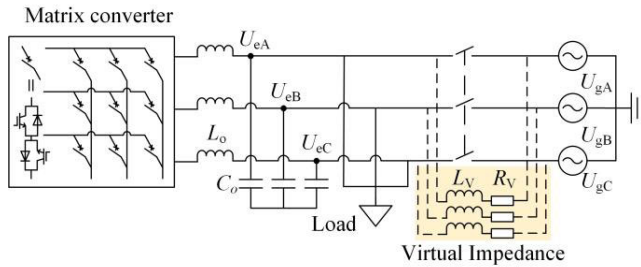


FIGURE 8. Virtual impedance-based system topology.

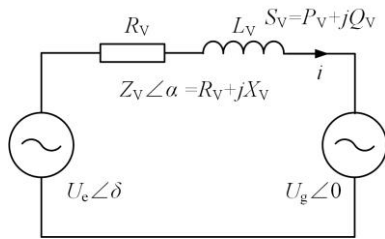


FIGURE 9. Equivalent model of grid-connected system.

modulation can realize no steady-state error of the system frequency in the islanded operation mode.

C. VIRTUAL POWER-BASED SYNCHRONIZATION CONTROL

Grid voltage synchronization should be achieved before connecting to the grid. Traditional synchronization control methods usually require an accurate PLL that can potentially threaten the system’s stability [22]. This paper investigates a virtual power-based synchronization control strategy without a PLL. The proposed synchronization strategy introduces a virtual impedance between the VSG-controlled generation system and the grid, as shown in Fig. 8. The virtual power-based synchronization control strategy adjusts the amplitude, frequency, and phase of the three-phase voltages of the VSG system according to the generated virtual power, thus achieving grid voltage synchronization and facilitating a smooth grid connection.

The grid-connected VSG system model can be equivalent to an ideal voltage source connected to the grid through the output impedance, as shown in Fig. 9.

In Fig. 9, U_e and U_g represent the amplitudes of the VSG system output voltage and the grid voltage respectively; δ is the phase difference between the VSG output voltage and the grid voltage; $Z_v \angle \alpha$ is the virtual impedance between the MC-based VSG power generation system and the grid. The virtual power delivered by the VSG power generation system to the grid through the virtual impedance is

$$\begin{aligned}
 S &= 3U_g I^* = 3U_g \frac{U_e \angle(-\delta) - U_g \angle 0}{Z_v \angle(-\alpha)} \\
 &= \frac{3U_e U_g}{Z_v} \angle(\alpha - \delta) - \frac{3U_g^2}{Z_v} \angle \alpha \\
 &= \left[\frac{3U_e U_g}{Z_v} \cos(\alpha - \delta) - \frac{3U_g^2}{Z_v} \cos \alpha \right] \\
 &\quad + j \left[\frac{3U_e U_g}{Z_v} \sin(\alpha - \delta) - \frac{3U_g^2}{Z_v} \sin \alpha \right] \\
 &= P_V + jQ_V
 \end{aligned} \tag{15}$$

and therefore:

$$\begin{cases} P_V = \frac{3U_e U_g}{Z_v} \cos[\alpha - \delta] - \frac{3U_g^2}{Z_v} \cos \alpha \\ Q_V = \frac{3U_e U_g}{Z_v} \sin[\alpha - \delta] - \frac{3U_g^2}{Z_v} \sin \alpha \end{cases} \tag{16}$$

It can be concluded from (16) that the virtual power delivered by the system to the grid is only related to the magnitude and phase of U_e if $U_e = U_g$ and $\delta = 0$. Under this condition, the virtual active power P_V and reactive power Q_V are both zero, and the voltage of the power generation system is the same as the grid voltage, which allows a smooth grid connection.

When designing the parameters of virtual impedance, one can refer to the approximate values of line impedance in practical applications of similar ratings. Since the generated current and power are virtual, it is possible to appropriately adjust the parameters. Reducing the value of the virtual impedance during the control process will increase the virtual current and virtual power, thereby accelerating the control process and vice versa. In addition, the virtual resistor and inductor form a low-pass filter that can remove the high-frequency harmonics in the measured voltage and thus reduce the harmonics in the calculated power.

To ensure that the amplitude of the power generation system output voltage is the same as the amplitude of the grid, a voltage amplitude compensation PI controller is adopted, as shown in the virtual power-based synchronization unit in Fig. 6.

The voltage phase compensation control unit is designed according to (16). The system output voltage phase is related to the system’s virtual active and reactive power, so the virtual active or reactive power can be used to adjust the system output voltage phase angle. In this paper, the virtual reactive power is used to design the voltage phase compensation control unit, and the control block diagram is shown in

TABLE 3. Simulation parameters.

Parameter	Value	Parameter	Value
L_s	5 mH	J	0.5 kg·m ²
R_s	30 Ω	K_q	0.00311
C_s	15 μF	K	20
U_m	800 V	U_{ref}	311 V
U_g	311 V	ω_0	314 rad/s
L_o	8 mH	K_i	800
C_o	15 μF	R_V	0.05 Ω
D	12.6651	L_V	0.2 mH

Fig. 10. The reactive power reference Q_{V_ref} is zero and the three-phase instantaneous reactive power is calculated by

$$Q_V = \left(1/\sqrt{3}\right) \times (u_{gAB} \times i_{gCV} + u_{gBC} \times i_{gAV} + u_{gCA} \times i_{gBV}) \tag{17}$$

A PI controller is used to generate $\Delta\omega_g$ to compensate for the system output frequency ω in the VSG system so that the system output voltage phase is synchronized with the phase of the grid voltage.

V. SIMULATION VERIFICATION

The MC-based VSG control strategy is modeled and simulated to verify the proposed control strategy. Simulation parameters are shown in Table 3.

A. VSG VERIFICATION IN ISLANDED MODE

The MC-interfaced power generation system is first operated in the islanded mode and the local load power is 25 kW during 0~1s and increased by 5 kW after 1 s. The system output power simulation waveform is shown in Fig. 11.

The MC-interfaced power generation system output voltages (u_{eA} , u_{eB} , u_{eC}) are shown in Fig. 12. As observed, the voltage amplitude is 311 V and the frequency is 50 Hz, which meets the load requirement.

The load power is increased by 5 kW at 1 s. The corresponding comparative waveforms of the system output frequency in the conventional droop control, the proposed VSG control, and the proposed VSG control with secondary frequency regulation are shown in Fig. 13.

As shown in Fig. 13, the system output frequencies in droop and VSG control have similar steady-state performance. In contrast, the frequency in droop control drops to 49.8 Hz immediately, taking about 15 ms, whereas the frequency in VSG control decreases to 49.8 Hz after about 0.3 s. It can be seen that the VSG control scheme provides inertia support for the system and significantly reduces the rate of change of the frequency. In the VSG with the secondary frequency regulation strategy, the system frequency gradually drops after the load change at 1 s. Then the system frequency is recovered to the rated value at around 1.1 s because of the introduced secondary frequency regulation, thus achieving

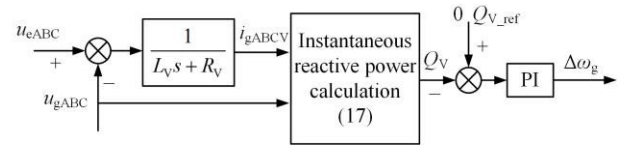


FIGURE 10. Virtual impedance-based system topology.

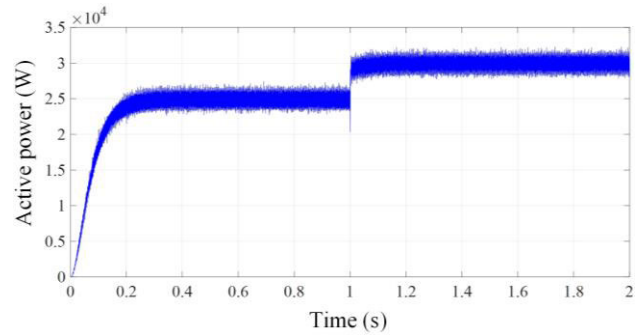


FIGURE 11. System output active power waveform.

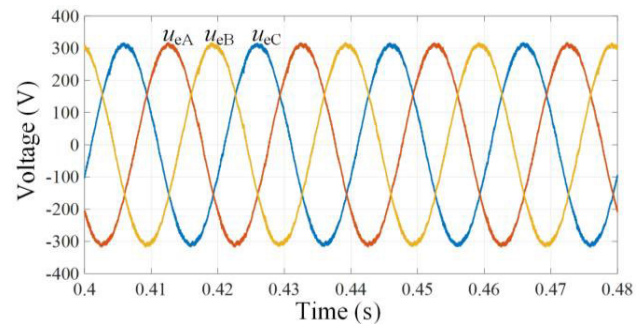


FIGURE 12. MC-interfaced power generation system output voltages.

no steady-state error in frequency regulation. In addition, the frequency only drops by 0.07 Hz in the transient process in the VSG with the secondary frequency regulation scheme, so the overall frequency response performance is enhanced.

The unity power factor at the MC input side is usually desired for efficient operation. The unity power factor control is achieved by the input current control unit in Fig. 6 and the simulation results are shown in Figs. 14 and 15. As observed, the source voltage and current are in phase and the source reactive power is zero.

The harmonics of the system output voltage and source current are analyzed and the results are shown in Figs. 16 and 17. The total harmonic distortion (THD) of the system output voltage is 1.54% and the THD of the source current is 3.60%.

B. VIRTUAL POWER-BASED SYNCHRONIZATION VERIFICATION

To achieve a seamless grid connection, the virtual power-based synchronization is initiated at 2 s. The simulation

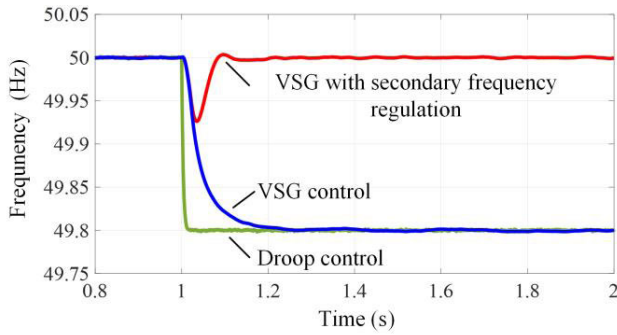


FIGURE 13. Comparative system output frequency waveform.

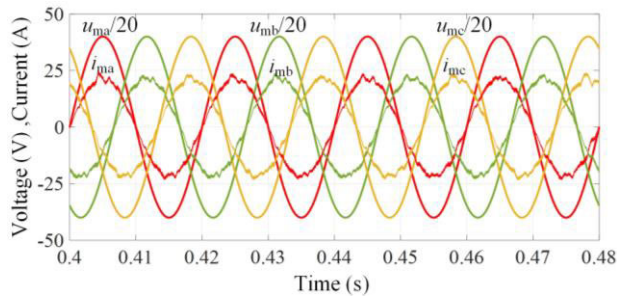


FIGURE 14. System source voltage and current waveform.

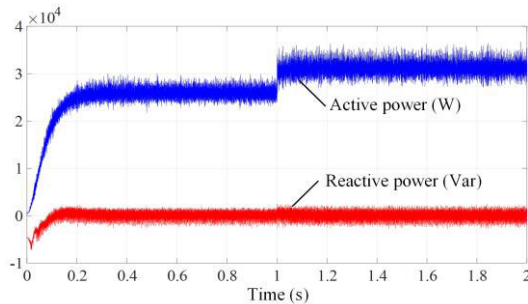


FIGURE 15. System source power waveform.

results of the grid voltage synchronization are shown in Figs. 18 and 19.

As previously described, a virtual impedance between the MC-interface generation system and grid is introduced in the proposed virtual power-based synchronization control strategy. The virtual power is controlled to be zero to achieve the grid voltage synchronization. As seen in Fig. 18, before synchronization, the virtual active and reactive powers are -870 kW and 375 kVar respectively, and then they approach zero after the synchronization control is activated at 2 s. At about 2.03 s, virtual active and reactive powers become zero, indicating that the grid voltage synchronization is achieved. As observed in the voltage synchronization process in Fig. 19, the system output voltage is synchronized with the grid voltage at about 2.03 s. These results demonstrate the effectiveness of the proposed virtual power-based synchronization strategy.

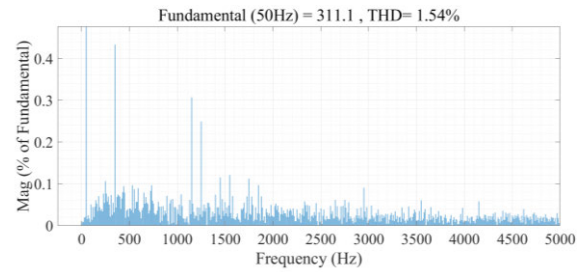


FIGURE 16. Harmonics in the system output voltage.

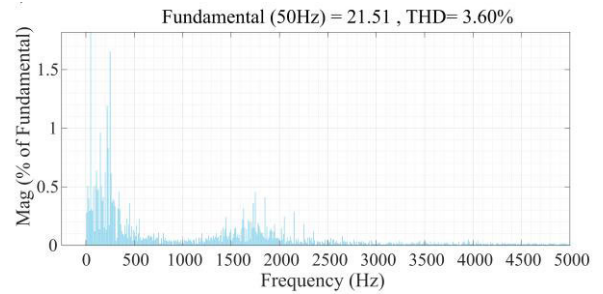


FIGURE 17. Harmonics in the source current.

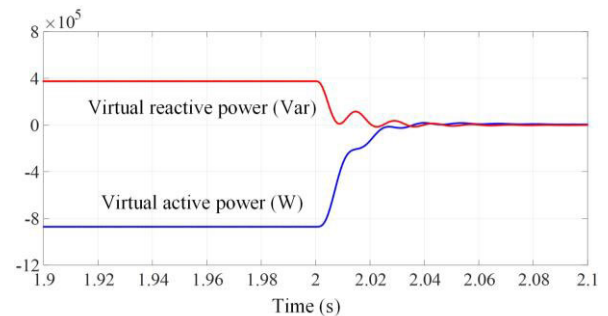


FIGURE 18. Output virtual power waveform.

The proposed virtual power-based synchronization strategy is compared with the conventional PLL-based synchronization and the comparative result is shown in Fig. 20.

As shown in Fig. 20, the difference between the system output voltage and the grid voltage in the traditional PLL-based synchronization technique tends to zero after 2.05 s, realizing the grid voltage synchronization. In contrast, the voltage error in the proposed virtual power-based synchronization method becomes zero at about 2.03 s, achieving faster synchronization.

C. GRID CONNECTION VERIFICATION

After grid voltage synchronization, the MC-interfaced generation system is connected to the grid and delivers 5 kW active power at 2.5 s, followed by 5 kVar reactive power command at 3s. Taking the 30 kW local load into account, the system generates 35 kW in total. The simulation results are shown in Fig. 21.

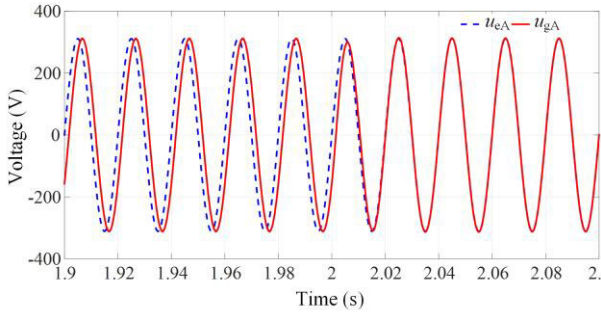


FIGURE 19. System voltage synchronizing with the grid voltage.

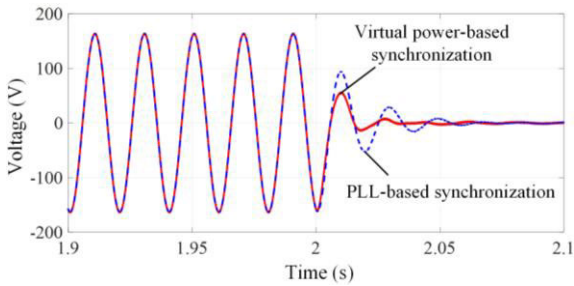


FIGURE 20. Error between the system output voltage and grid voltage during synchronization.

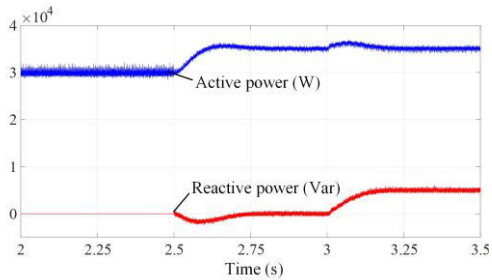


FIGURE 21. System output power after grid connection.

As shown in Fig. 21, a smooth grid connection is realized. After the grid connection, the system output power can be effectively controlled to follow the power command to deliver the power to the local load and grid.

D. VERIFICATION UNDER SOURCE VARIATIONS

To verify that the proposed grid-forming control strategy can still provide virtual inertia and damping where variations occur in the input, input frequency fluctuations are added to simulate the fluctuations and intermittency of new energy power generation systems. The input source voltage amplitude has $\pm 5\%$ fluctuations around 800 V, as shown in Fig. 22, while the frequency fluctuates between 49.5 Hz and 50.5 Hz, as shown in Fig. 23.

Figs. 24 and 25 represent the comparative simulation waveforms of MC-interfaced generation system output voltage and frequency controlled by droop control and VSG control.

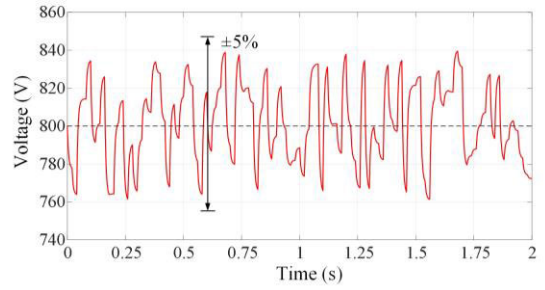


FIGURE 22. Source voltage fluctuations.

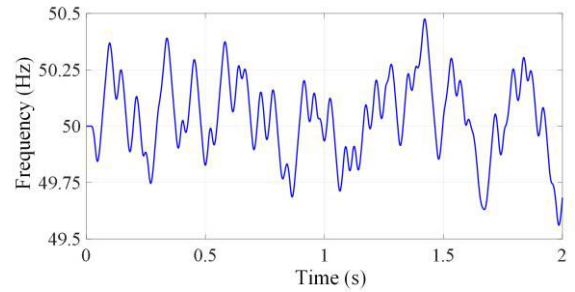


FIGURE 23. Source frequency variations.

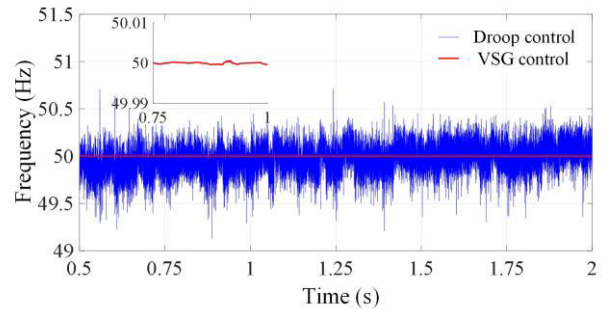


FIGURE 24. MC-interfaced power generation system output frequency under source variations.

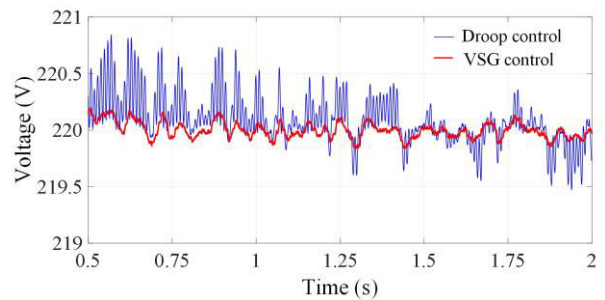


FIGURE 25. MC-interfaced power generation system output voltage under source variations.

As shown in Fig. 24, even when the input source voltage and frequency fluctuate, the MC-interfaced system output frequency regulated by the VSG remains at 50 Hz, whereas

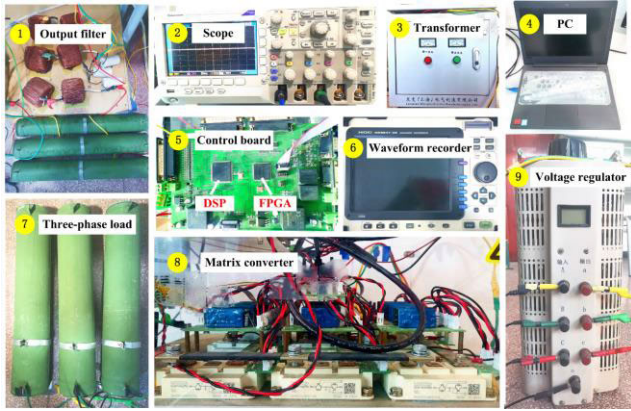


FIGURE 26. Experimental setup.

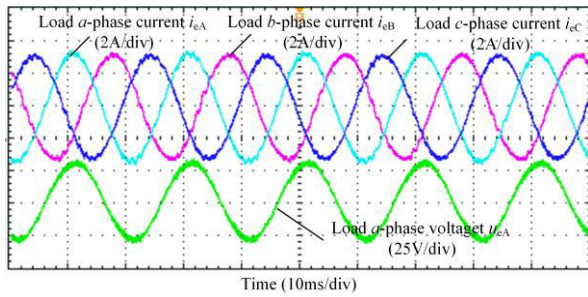


FIGURE 27. Experimental waveforms of system output voltages and current.

the frequency in the droop control fluctuates between 49.5 Hz and 50.5 Hz, exhibiting considerable variations.

As shown in Fig. 25, the maximum deviation of the MC-interfaced power generation system output voltage regulated by the VSG control is about 0.2 V. However, in the droop control method, the voltage deviation reaches up to 0.8 V.

From the above results, it can be concluded that in comparison with the traditional droop control, the VSG-based grid-forming control strategy proposed in this paper is capable of providing inertia and damping support to maintain the system output voltage and frequency.

VI. EXPERIMENTAL VERIFICATION

In order to further verify the correctness and effectiveness of the proposed control strategies, an experimental platform based on TMS320F28335 DSP and Altera Cyclone I FPGA has been built. The experimental setup is shown in Fig. 26. The experimental parameters are shown in Table 4.

A. VSG VERIFICATION IN ISLANDED MODE

In islanded mode, the MC-interfaced generation system outputs 135 W active power and 0 Var reactive power supplying the local load. The steady-state experimental waveforms are shown in Figs. 27 and 28.

Fig. 27 shows the experiment waveforms of the system output three-phase current and the a-phase voltage. As seen in Fig. 27, the system output voltages and currents are sinusoidal

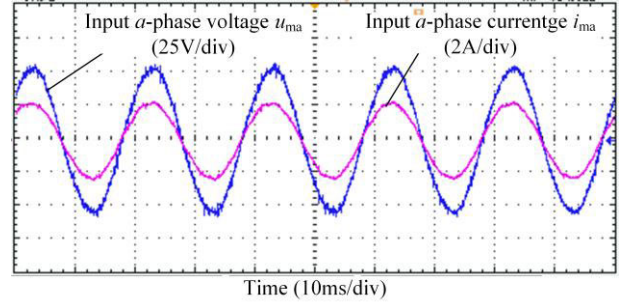


FIGURE 28. Experimental waveforms of source a-phase voltage and current.

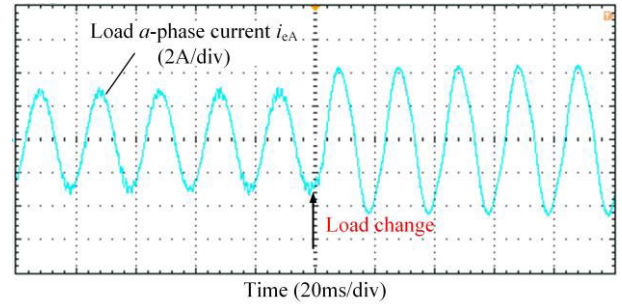


FIGURE 29. Experimental waveform of load a-phase current in response to load change.

TABLE 4. Experimental parameters.

Parameter	Value	Parameter	Value
L_s	10 mH	U_m	50 V
C_s	30 μ F	U_o	30 V
R_s	20 Ω	U_g	30 V
L_o	10 mH	T_s	10 0 μ s
C_o	10 μ F	K_i	0.2
D	0.1	J	0.01
K_q	0.01	K	0.1
R_v	0.05 Ω	L_v	0.2 mH

and can supply the load effectively. The a-phase voltage u_{eA} is in phase with the current i_{eA} , so the output reactive power is zero. Fig. 28 shows the experimental waveforms of the source phase a-voltage and current. As seen in Fig. 28, the amplitude of the source a-phase voltage u_{ma} is 50 V and the amplitude of the current i_{ma} is 2 A. The source voltage and current are in phase, verifying the unity power factor operation. Figs. 29 and 30 demonstrate the steady-state performance of the proposed method in the islanded mode.

To verify the transient performance of the proposed control strategy, the load power is increased by 67.5 W and the corresponding experimental results are shown in Figs. 29-31.

Fig. 29 shows the experimental waveform of a-phase load current, from which the current is increased from 3 A to 4.5 A in response to the load change. Fig. 30 shows the corresponding experimental system frequency waveform for

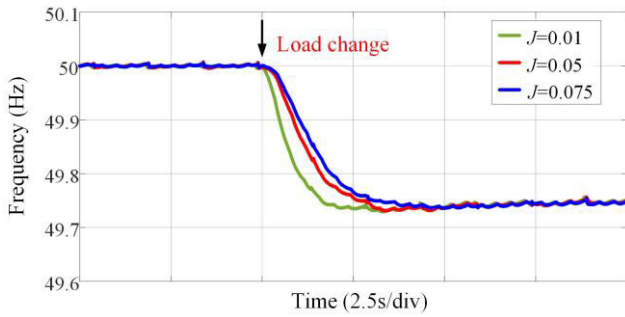


FIGURE 30. Experimental waveform of system frequency in response to load change.

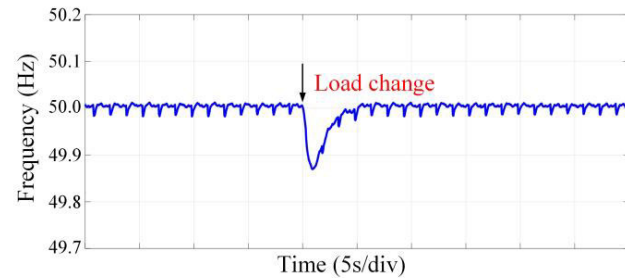


FIGURE 31. Experimental waveform of system frequency in the VSG with secondary frequency regulation.

$D = 0.1$ and $J = 0.01, 0.05, 0.0075$. As seen in Fig. 30 with the proposed VSG control scheme, the frequency in the MC-interfaced generation system exhibits characteristics similar to the synchronous generator. Inertia and damping effects are observed in the frequency waveform and they can beneficially support the system frequency when needed. It can be concluded from Fig. 30 that the larger the virtual inertia, the more significant the inertia effect observed in the frequency waveform. However, the system frequency changes from the rated 50 Hz to about 49.75 Hz and there is an obvious steady-state error in the frequency regulation.

Fig. 31 shows the experimental system frequency in the proposed VSG scheme with the secondary frequency regulation. As observed in Fig. 31, the system frequency drops slightly when the load changes and then is restored to the rated 50 Hz.

B. VIRTUAL POWER-BASED SYNCHRONIZATION VERIFICATION

The comparative experimental waveform of voltage error in the synchronization process between the traditional PLL-based synchronization method and the proposed virtual power-based synchronization method are shown in Figs. 32 and 33.

When the control command is given, the system output voltage is gradually synchronizing with the grid voltage, resulting in the error between the system voltage and grid voltage decreasing gradually, as seen in Fig. 32. It takes about 300 ms for the voltage error to become zero, thus realizing

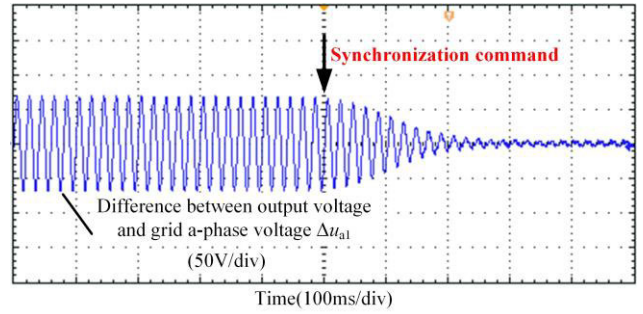


FIGURE 32. Experimental waveform of the error between the system voltage and grid voltage in the PLL-based synchronization process.

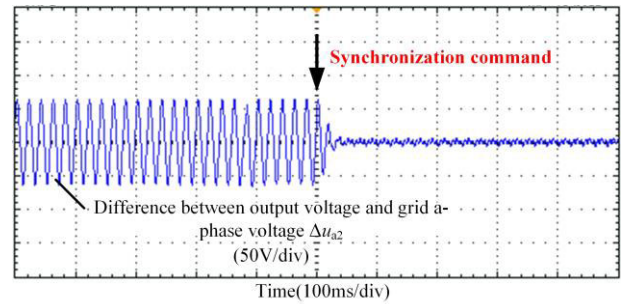


FIGURE 33. Experimental waveform of the error between the system voltage and grid voltage in the proposed virtual power-based synchronization process.

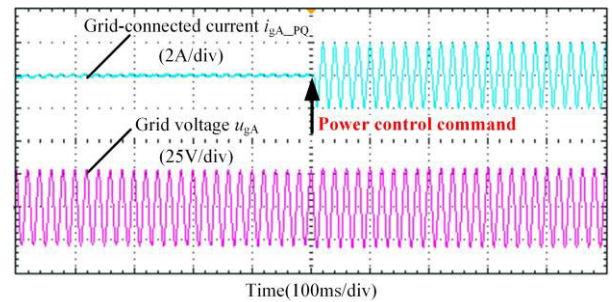


FIGURE 34. Experimental grid current and voltage in the PQ control scheme.

grid synchronization. In contrast, it only takes about 50 ms for the system voltage to be synchronized with the grid voltage in the proposed virtual power-based synchronization method, as indicated in Fig. 33. Therefore, it can be concluded that the proposed virtual power-based synchronization method can achieve faster grid synchronization without PLL.

C. CONNECTION VERIFICATION

After the grid synchronization is achieved, the MC-interfaced generation system can be connected to the grid and the grid-connected power control can be implemented. In the grid-connected mode, the power command is 90 W. The performance of the proposed VSG strategy is compared with the conventional PQ control method in the grid-connected mode. The comparative results are shown in Figs. 34 and 35.

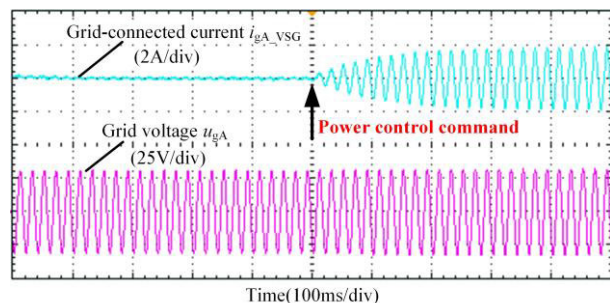


FIGURE 35. Experimental grid-connected current and voltage in the VSG control strategy.

The experimental results of grid-connected current and voltage regulated by the traditional PQ control scheme are shown in Fig. 34. As seen in Fig. 34, the grid-connected current increased instantly when the 90 W power control command was given. The power control command can be effectively fulfilled, but there is no inertia or damping characteristic. In contrast, with the proposed VSG method, the MC-interfaced generation system demonstrates desirable inertia and damping characteristics similar to the synchronous generation, as observed in the experimental waveforms shown in Fig. 35. The beneficial inertia and damping effect are advantageous to the integration of renewable power generation system, facilitating a friendly grid connection.

VII. CONCLUSION

VSG technology can enable the power electronic converter-interfaced renewable power generation system to mimic the traditional synchronous generation and exhibit beneficial inertia and damping characteristics. However, the VSG control for the MC is rarely reported in the literature. This paper investigates the VSG control of the grid-forming MC used as an interface converter in the AC source distributed generation system. A secondary frequency regulation is introduced to achieve the frequency regulation without steady-state error. A virtual power-based synchronization is investigated to synchronize the system output voltage with the grid voltage to facilitate a smooth grid connection. The VSG-based power control is implemented in the grid-connected mode. Simulation and experimental results verify the effectiveness of the proposed control strategies. The research described in this paper develops the control of grid-forming MC, and more research effort should be devoted to this topic to promote the grid connection of the MC-interfaced AC source distributed generation system.

REFERENCES

- [1] F. Blaabjerg, R. Teodorescu, M. Liserre, and A. V. Timbus, "Overview of control and grid synchronization for distributed power generation systems," *IEEE Trans. Ind. Electron.*, vol. 53, no. 5, pp. 1398–1409, Oct. 2006.
- [2] M. H. Saeed, W. Fangzong, B. A. Kalwar, and S. Iqbal, "A review on microgrids' challenges & perspectives," *IEEE Access*, vol. 9, pp. 166502–166517, 2021.
- [3] J. Liu, Y. Miura, and T. Ise, "Comparison of dynamic characteristics between virtual synchronous generator and droop control in inverter-based distributed generators," *IEEE Trans. Power Electron.*, vol. 31, no. 5, pp. 3600–3611, May 2016.
- [4] A. Fernández-Guillamón, E. Gómez-Lázaro, E. Muljadi, and Á. Molina-García, "Power systems with high renewable energy sources: A review of inertia and frequency control strategies over time," *Renew. Sustain. Energy Rev.*, vol. 115, Nov. 2019, Art. no. 109369.
- [5] J. I. Sarasua, G. Martínez-Lucas, H. García-Pereira, G. Navarro-Soriano, Á. Molina-García, and A. Fernández-Guillamón, "Hybrid frequency control strategies based on hydro-power, wind, and energy storage systems: Application to 100% renewable scenarios," *IET Renew. Power Gener.*, vol. 16, no. 6, pp. 1107–1120, Apr. 2022.
- [6] B. Kroposki, B. Johnson, Y. Zhang, V. Gevorgian, P. Denholm, B.-M. Hodge, and B. Hannegan, "Achieving a 100% renewable grid: Operating electric power systems with extremely high levels of variable renewable energy," *IEEE Power Energy Mag.*, vol. 15, no. 2, pp. 61–73, Mar. 2017.
- [7] Q.-C. Zhong and G. Weiss, "Synchronverters: Inverters that mimic synchronous generators," *IEEE Trans. Ind. Electron.*, vol. 58, no. 4, pp. 1259–1267, Apr. 2011.
- [8] M. Poursmaeil, R. Sangrody, S. Taheri, and E. Poursmaeil, "An adaptive parameter-based control technique of virtual synchronous generator for smooth transient between islanded and grid-connected mode of operation," *IEEE Access*, vol. 9, pp. 137322–137337, 2021.
- [9] J. Liu, Y. Miura, H. Bevrani, and T. Ise, "Enhanced virtual synchronous generator control for parallel inverters in microgrids," *IEEE Trans. Smart Grid*, vol. 8, no. 5, pp. 2268–2277, Sep. 2017.
- [10] J. Fang, Y. Tang, H. Li, and X. Li, "A battery/ultracapacitor hybrid energy storage system for implementing the power management of virtual synchronous generators," *IEEE Trans. Power Electron.*, vol. 33, no. 4, pp. 2820–2824, Apr. 2018.
- [11] X. Quan, R. Yu, X. Zhao, Y. Lei, T. Chen, C. Li, and A. Q. Huang, "Photovoltaic synchronous generator: Architecture and control strategy for a grid-forming PV energy system," *IEEE J. Emerg. Sel. Topics Power Electron.*, vol. 8, no. 2, pp. 936–948, Jun. 2020.
- [12] M. Mao, C. Qian, and Y. Ding, "Decentralized coordination power control for islanding microgrid based on PV/BES-VSG," *CPSS Trans. Power Electron. Appl.*, vol. 3, no. 1, pp. 14–24, Mar. 2018.
- [13] S. Sang, C. Zhang, X. Cai, M. Molinas, J. Zhang, and F. Rao, "Control of a type-IV wind turbine with the capability of robust grid-synchronization and inertial response for weak grid stable operation," *IEEE Access*, vol. 7, pp. 58553–58569, 2019.
- [14] Q.-C. Zhong, Z. Ma, W.-L. Ming, and G. C. Konstantopoulos, "Grid-friendly wind power systems based on the synchronverter technology," *Energy Convers. Manage.*, vol. 89, pp. 719–726, Jan. 2015.
- [15] Y. Ma, W. Cao, L. Yang, F. Wang, and L. M. Tolbert, "Virtual synchronous generator control of full converter wind turbines with short-term energy storage," *IEEE Trans. Ind. Electron.*, vol. 64, no. 11, pp. 8821–8831, Nov. 2017.
- [16] J. Zhang, L. Li, and D. G. Dorrell, "Control and applications of direct matrix converters: A review," *Chin. J. Electr. Eng.*, vol. 4, no. 2, pp. 18–27, Jun. 2018.
- [17] J. Zhang, L. Li, D. G. Dorrell, M. Norambuena, and J. Rodriguez, "Predictive voltage control of direct matrix converters with improved output voltage for renewable distributed generation," *IEEE J. Emerg. Sel. Topics Power Electron.*, vol. 7, no. 1, pp. 296–308, Mar. 2019.
- [18] J. Zhang, H. Chang, T. He, N. Zhang, and G. Liu, "Virtual synchronous generator controlled matrix converter for grid integration in distributed generation and microgrid," in *Proc. 8th Renew. Power Gener. Conf.*, 2019, pp. 1–6.
- [19] C. Li, Y. Guo, W. Deng, and X. Wang, "Matrix converter based virtual synchronous generation technology," *J. Eng.*, vol. 2019, no. 16, pp. 1972–1975, Mar. 2019.
- [20] H. Wang, J. Zhang, and G. Liu, "Virtual synchronous generator control strategy based on matrix converter," in *Proc. 3rd New Energy Energy Storage Syst. Control Summit Forum (NESSC)*, Mianyang, China, Sep. 2023, pp. 473–477.
- [21] H. Li, K. Meng, Y. Peng, and X. Li, "Control strategy for seamless switching of virtual synchronous generators based on secondary frequency and voltage regulation," *Alexandria Eng. J.*, vol. 61, no. 12, pp. 10477–10484, Dec. 2022.

- [22] Q.-C. Zhong, P.-L. Nguyen, Z. Ma, and W. Sheng, "Self-synchronized synchronverters: Inverters without a dedicated synchronization unit," *IEEE Trans. Power Electron.*, vol. 29, no. 2, pp. 617–630, Feb. 2014.



JIANWEI ZHANG (Member, IEEE) received the bachelor's degree in electrical engineering from Northwest A&F University, Shaanxi, China, in 2014, and the Ph.D. degree in electrical engineering from the University of Technology Sydney (UTS), Sydney, Australia, in 2018. He was a Casual Academic with the Faculty of Engineering and IT, UTS, from 2015 to 2018. In 2018, he joined Inner Mongolia University of Technology (IMUT), Hohhot, China, where he is currently an Associate Professor with the College of Electric Power. He was a Visiting Scholar with the Power Electronics, Machines and Control (PEMC) Research Group, Faculty of Engineering, University of Nottingham, U.K., from 2022 to 2023. His research interests include matrix converters, microgrids, energy storage, and ac motor drives.



HUIDONG WANG received the bachelor's degree in electrical engineering from Inner Mongolia University of Technology, China, in 2021, where he is currently pursuing the master's degree in electrical engineering. His research interests include matrix converter and control.



GUANGCHEN LIU (Member, IEEE) received the bachelor's degree in power system automation from Inner Mongolia University of Technology (IMUT), China, in 1999, the master's degree in control theory and engineering from Beijing Institute of Technology, China, in 2006, and the Ph.D. degree in power machinery and engineering from IMUT, in 2012. From July 2017 to August 2018, he was a Visiting Scholar with the University of Strathclyde, U.K. He is currently a Full Professor and the Dean of the College of Electric Power, IMUT. His research interests include control of renewable power generation and energy storage systems.



GUIZHEN TIAN received the B.S. degree in industrial automation, the M.S. degree in control theory and control engineering, and the Ph.D. degree in power machinery and engineering from Inner Mongolia University of Technology (IMUT), Hohhot, China, in 1998, 2002, and 2012, respectively. She is currently a Professor with IMUT. Her research interests include control technology of renewable energy generation, power electronics, and motion control.



MARCO RIVERA (Senior Member, IEEE) received the Electronic Civil Engineering degree and the M.Sc. degree in engineering, with specialization in electrical engineering from the Universidad de Concepción, and the Ph.D. degree in electronic engineering from the Universidad Técnica Federico Santa María.

He has been a Visiting Professor with several international universities. He was a Full Professor with the Department of Electrical Engineering, Universidad de Talca. Since April 2023, he has been with the Power Electronics, Machines and Control (PEMC) Research Group, University of Nottingham, as a Professor. He is currently the Director of the Laboratory of Energy Conversion and Power Electronics [Laboratorio de Conversión de Energías y Electrónica de Potencia, (LCEEP)], Universidad de Talca, Chile. He has published more than 520 academic publications in leading international conferences and journals. He has directed and participated in several projects financed by the National Fund for Scientific and Technological Development [Fondo Nacional de Desarrollo Científico y Tecnológico (FONDECYT)], the Chilean National Agency for Research and Development [Agencia Nacional de Investigación y Desarrollo (ANID)], and the Paraguayan Program for the Development of Science and Technology [Proyecto Paraguayo para el Desarrollo de la Ciencia y Tecnología (PROCIENCIA)]. He has been the responsible researcher of basal financed projects whose objective is to enhance, through substantial and long-term financing, Chile's economic development through excellence and applied research. His research interests include power electronics, renewable energies, advanced control of power converters, and microgrids. He was awarded the "Premio Tesis de Doctorado Academia Chilena de Ciencias 2012," for the Best Ph.D. Thesis developed in 2011 for national and foreign students in any exact or natural sciences program, that is member of the Academia Chilena de Ciencias, Chile.



PATRICK WHEELER (Fellow, IEEE) received the B.Eng. degree (Hons.) and the Ph.D. degree in electrical engineering for his work on matrix converters from the University of Bristol, U.K., in 1990, in 1994, respectively.

In 1993, he moved to the University of Nottingham and was a Research Assistant with the Department of Electrical and Electronic Engineering. In 1996, he became a Lecturer with the Power Electronics, Machines and Control Group, University of Nottingham, U.K., where he has been a Full Professor, since January 2008. He was the Head of the Department of Electrical and Electronic Engineering, University of Nottingham, from 2015 to 2018. He is currently the Global Engagement Director of the Faculty of Engineering, the Head of the Power Electronics, Machines and Control Research Group, and the Director of the Institute of Aerospace Technology, University of Nottingham. He has published more than 850 academic publications in event leading international conferences and journals. He is a member of the IEEE PELS AdCom and also the IEEE PELS Vice-President of Technical Operations.

• • •